physica status solidi

pss

www.interscience.wiley.com

reprints

www.pss-rapid.com

www.pss-c.com

www.pss-b.com

www.pss-a.com

WILEY-VCH

REPRINT

Phys. Status Solidi B **247**, No. 7, 1814–1821 (2010) / **DOI** 10.1002/pssb.200945416

physica status solidi b
www.pss-b.com
basic solid state physics

Ab initio calculations of optical spectra of a chiral (4,1) carbon nanotube

T. Movlarooy[1,2], S. M. Hosseini*[,1], A. Kompany[1], and N. Shahtahmasebi[1]

[1] Department of Physics, Ferdowsi University of Mashhad (Materials and Electroceramics Laboratory), Mashhad, Iran
[2] Department of Physics, Shahrood University of Technology, Shahrood, Iran

Received 5 September 2009, revised 17 January 2010, accepted 10 February 2010
Published online 22 March 2010

Keywords carbon nanotubes, DFT, optical properties

* Corresponding author: e-mail sma_hosseini@yahoo.com, Phone: +98511 8435723, Fax: +98511 8796416

We report *ab initio* calculations of electronic and the linear optical properties of a (4,1) chiral carbon nanotube, using the full-potential linear augmented plane-wave (FP-LAPW) method. The dielectric tensor is derived within the random-phase approximation (RPA). All optical spectra, such as: dielectric function, absorption coefficient, optical conductivity, extinction coefficient, loss function, sum rule, reflectivity, and the refractive index have been calculated for both electric field polarizations, parallel and perpendicular to the tube axis. It is revealed that the optical spectra are anisotropic along these two polarizations. For the parallel polarization, adding the intraband transition contributions, will change the optical spectra of a (4,1) nanotube significantly. The calculated optical gap, E_g, electronic dielectric constant, $\varepsilon(\infty)$, and the refractive index, n, in the parallel polarization are obtained as 2.6 eV, 1.98, and 1.4, respectively. The results show that for small diameter of SWCNTs the chirality has a strong effect on their optical spectra. Adding the intraband transition contributions showed that the dielectric function has singularity at zero frequency, due to the metallic behavior of a (4,1) chiral nanotube.

© 2010 WILEY-VCH Verlag GmbH & Co. KGaA, Weinheim

1 Introduction Since the discovery of carbon nanotubes (CNTs) in 1991, the fabrication of nanometer-scaled one-dimensional materials has attracted considerable interest due to their potential use in both nanotechnology and nanoscale engineering [1]. The stability and quasi-one-dimensional nature of single-walled carbon nanotubes (SWCNTs) make them unique systems from the experimental and theoretical points of view. Because of the one-dimensional character and chirality, chiral CNTs are expected to exhibit a number of unusual optical properties: such as optical rotation, circular dichroism, and second-harmonic generation [2–5].

SWCNTs, and in particular small-diameter SWCNTs, have attracted broad interest due to their unique electronic structure and properties. The small-diameter nanotubes exhibit either metallic or semiconducting behavior, depending strongly on the tube diameters and chiralities [6, 7]. The optical properties reflect the electronic energy band structures of materials and have a close relation with their geometrical structures, especially for the nanosized materials. In addition, the optical responses of SWCNTs are useful to characterize these nanotubes and can be employed in device applications [8].

Recent advances in the measurement of the optical properties of individual SWCNTs [8–11] have generated a great deal of interest and provided a wealth of information. The smallest CNT (2,2) has been studied experimentally by Zhao et al. [12], Thang et al. [13], and theoretically by Scipioni [14]. Deslippe et al. [15] have presented an *ab initio* calculation on excitonic effects in metallic SWCNTs with larger diameter. However, there are a lot of theoretical and experimental works on the optical properties of zigzag SWCNTs, but due to the low symmetry of chiral SWCNTs these systems have only rarely been considered.

In this study we have used the random-phase approximation (RPA) to obtain the optical spectra and the effect of many-electron interactions such as excitonic effects have been neglected. In a few interesting papers quasiparticle formalisms have been used and predicted the optical transitions of small SWCNTs in agreement with experimental data [16, 17]. Further more, Marinopoulos et al. [18, 19] used time-dependent density functional theory (TD-DFT) on small-diameter SWCNTs and concluded that for the electric field polarized parallel to the tube axis the local field effects and induced exchange correlation components, beyond the RPA, are negligible.

WILEY InterScience DISCOVER SOMETHING GREAT

© 2010 WILEY-VCH Verlag GmbH & Co. KGaA, Weinheim

We have carried out a first-principle calculations on a small-diameter (4,1) CNT with 3.6 Å diameter. We are not aware of any published experimental or theoretical data for this special CNT, so our calculation can be used to cover this lack of data.

2 Computational details All calculations presented in this work are based on DFT [20]. The Perdew–Burke–Ernzerhof generalized gradient approximation (GGA) was used for the exchange correlation correction [21, 22]. The density of states (DOS) is deduced from a self-consistent calculation, using the full-potential linearized augmented plane wave (FP-LAPW) method and the dielectric function is obtained by the RPA, as embodied in the Wien2k Code [23]. The convergence of the basis set is controlled by a cut off parameter $R_m \times k_{max} = 6$. The values of other parameters are $G_{max} = 12$ (magnitude of largest vector in charge density Fourier expansion or the plane wave cutoff), $R_{MT}(C) =$ 1.28 au (muffin-tin radius). The iteration halted when the difference in charge was less than 0.000001e between steps as the convergence criterion. The optical spectra were calculated using 80 k-points in the first Brillouin zone and setting the Lorentzian broadening with gamma equal to 0.05 eV.

3 Results and discussions

3.1 Electronic structure The calculated electronic band structure and DOS for a (4,1) chiral nanotube are shown in Fig. 1. The band structure was calculated in the *x*-direction, since the periodicity of the tube is in this direction, as seen in Fig. 2. The electronic band structure and DOS show that a (4,1) nanotube is metallic with zero band gap and the valence and conduction bands cross each other at the Fermi level.

Due to the one-dimensional nature of the electronic bands, the DOS of SWNTs exhibits a series of characteristics. The van Hove singularities (vHs) at the onset of one-dimensional energy bands near the Fermi energy (E_f) can be seen in Fig. 1a. These vHs are asymmetric about E_f, due to the strong curvature effects. The arrows in Figs. 1a and b indicate the optically allowed interband transitions between the valence and conduction states that give rise to the three peaks, labeled A, B, and C in the optical spectrum shown in Fig. 3b. For a (4,1) metallic tube, the bands forming the first vHs below E_f and the second vHs above E_f cross each other about the Fermi level, but optical transitions between them are symmetry forbidden.

The peak splitting in the DOS diagram that is due to the trigonal warping effect is dependent on the diameter of nanotube for metallic nanotubes. [24]. In this reference the separation width of the first DOS peaks for (10,10) armchair is almost zero and increases with decrease in chiral angle nanotubes.

It seems for the small nanotube that the splitting width peaks in energy are not very clear in the DOS diagram when calculated by first principles, as there are many peaks. This effect has also not been reported and detected in the DOS diagram for other chiral nanotubes with metallic character, which has been performed by first-principles calculations [25].

From the DOS diagram, it is obvious that the valence and conduction bands are not symmetric (in contrast with tight

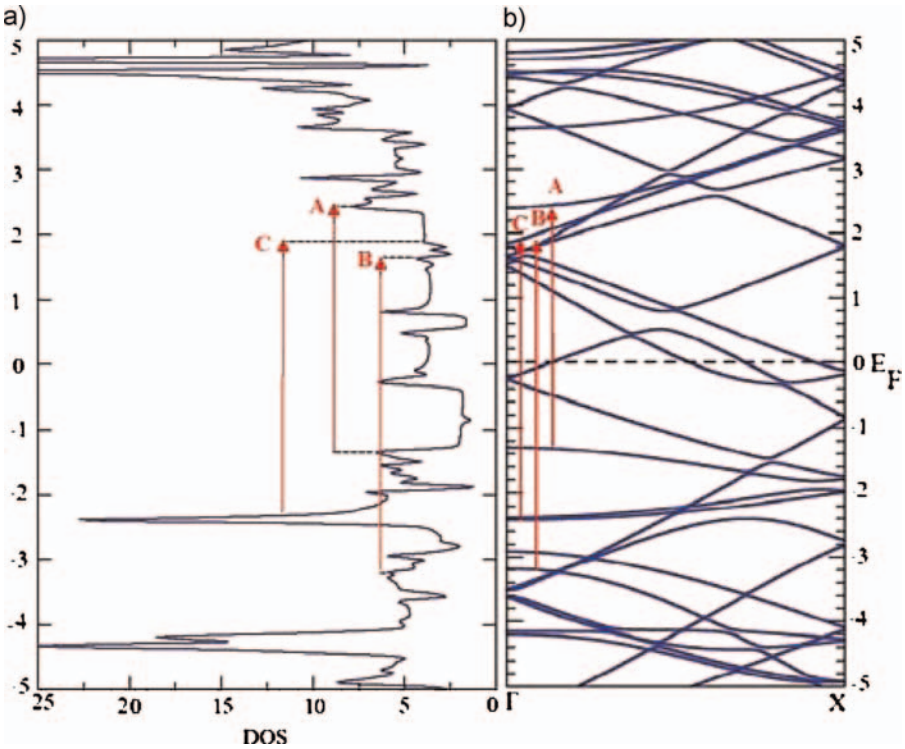

Figure 1 (online colour at: www.pss-b.com) (a) The DOS and (b) the electronic band structure of a (4,1) nanotube.

© 2010 WILEY-VCH Verlag GmbH & Co. KGaA, Weinheim

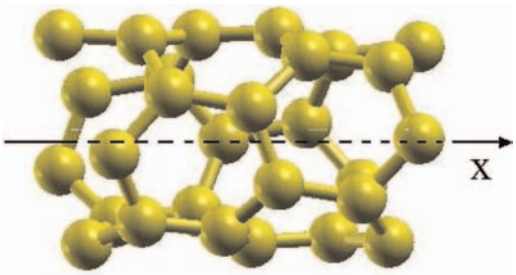

Figure 2 (online colour at: www.pss-b.com) Chiral (4,1) nanotube, periodicity of the tube is in the x-direction.

binding calculations). It seems that the π band is shifted down mainly due to the curvature effects.

3.2 Optical properties The optical properties of CNTs were studied experimentally by optical ellipsometry [26], electron energy-loss spectroscopy [27], reflectivity measurements [28], and absorption experiments [29]. The imaginary part of the dielectric tensor can be computed from the knowledge of the electronic band structure of a solid.

In the limit of linear optics, in the case of nonspin polarized, and within the frame of RPA we can use the following well-known relations [30]

$$\mathrm{Im}\varepsilon_{\alpha\beta}^{\{\mathrm{inter}\}}(\omega) = \frac{\hbar^2 e^2}{\pi m^2 \omega^2} \sum_{c,v} \int \mathrm{d}k \langle c_k|p^\alpha|v_k\rangle\langle v_k|p^\beta|c_k\rangle \times \delta(\varepsilon_{ck} - \varepsilon_{vk} - \omega). \quad (1)$$

The absorption spectrum is proportional to the sum over interband transitions from occupied valence (v_k) to empty conduction (c_k) states over the Brillouin-zone k points. From the imaginary part of the dielectric tensor component the corresponding real part is obtained by the Kramers–Kronig transformation:

$$\mathrm{Re}\varepsilon_{\alpha\beta}(\omega) = \delta_{\alpha\beta} + \frac{2}{\pi} P \int_0^\infty \frac{\omega' \mathrm{Im}\varepsilon_{\alpha\beta}(\omega')}{\omega'^2 - \omega^2} \mathrm{d}\omega'. \quad (2)$$

By adding the intraband contribution, in the case for metal, we would have [31]:

$$\mathrm{Im}\varepsilon_{\alpha\beta}^{[\mathrm{intra}]}(\omega) = \frac{\Gamma \omega_{\mathrm{pl},\alpha\beta}^2}{\omega(\omega^2 + \Gamma^2)}, \quad (3)$$

$$\mathrm{Re}\varepsilon_{\alpha\beta}^{[\mathrm{intra}]}(\omega) = 1 - \frac{\omega_{\mathrm{pl},\alpha\beta}^2}{\omega(\omega^2 + \Gamma^2)}, \quad (4)$$

where Γ is the lifetime broadening and ω_{pl} is the plasma frequency.

The real and imaginary parts of the dielectric function of a chiral (4,1) nanotube, considering the interband transitions for both polarizations, the electric field polarized parallel and perpendicular to the nanotube axis, are shown in Figs. 3a and b, respectively.

The value of electronic dielectric constant, $\varepsilon(\infty)$, in the parallel polarization is 1.98. This constant describes the effects of polarization of core states, σ and π bands except those lying near the Fermi level, and materials surrounding the nanotube. In nanotubes, this simple constant screening is a rough approximation because of the cylindrical form with a hollow vacuum inside and surrounding material outside.

The results for the imaginary part of the dielectric function of a (4,1) nanotube indicate some peaks that are related to the optical transitions. This can be explained from the occurrence of direct interband transitions between the vHs of the DOS. The calculated first, second, and third peak positions of a small-diameter (4,1) CNT are shown in Table 1, as indicated in Fig. 3b. The larger curvatures give rise to the larger hybridizations. However, the 3–4 Å nanotubes are the smallest nanotubes and have the largest curvature, thus having the strongest hybridization. This effect can be seen from the band structure (Fig. 1b). For the parallel polarization, the first peak occurs at energy about 2.6 eV.

Since there is no previous measurements on a chiral (4,1) nanotube with 3.6 Å diameter, we have to compare our

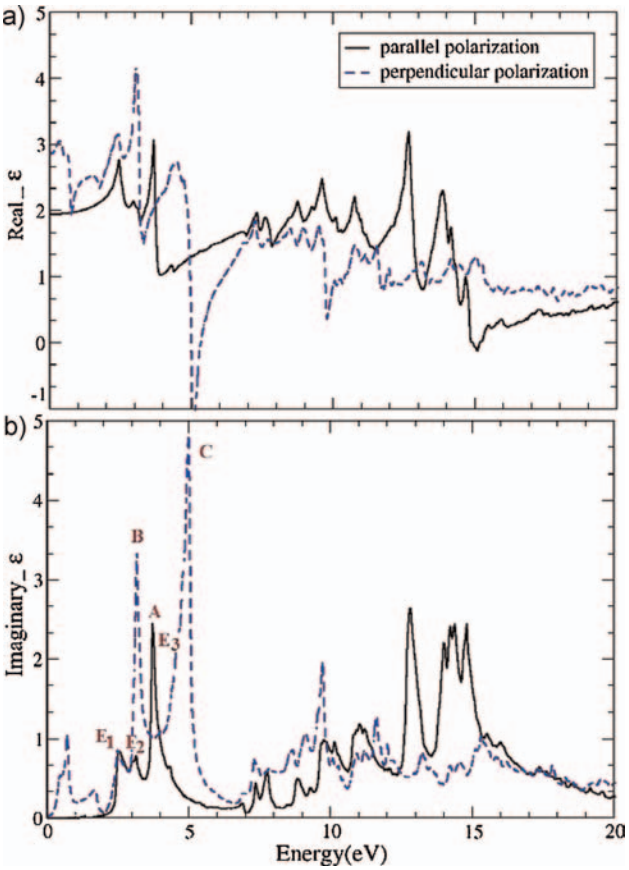

Figure 3 (online colour at: www.pss-b.com) (a) Real and (b) imaginary parts of the dielectric function for polarizations parallel and perpendicular to the tube axis.

© 2010 WILEY-VCH Verlag GmbH & Co. KGaA, Weinheim

Table 1 First, second, and third peak positions in a (3.6 Å) small-diameter (4,1) nanotube for the parallel polarization.

transition	E_1	E_2	E_3
energy (eV)	2.6	3.2	3.8

results with small-diameter 4 Å SWCNTs. Table 2 shows the theoretical and experimental measurements of first optical transitions of 3–4 Å SWCNTs. We have also calculated the electronic and optical properties of (3,3) and (4,2) nanotubes, but the details of the calculations are not given in this paper.

These results show that for small diameter of SWCNTs the chirality has a strong effect on their optical transitions and optical spectra. Table 2 also indicates that the optical gaps of small-diameter CNTs scale inversely with the tube length.

Labels A, B, and C indicate the highest absorption peaks observed in the low-energy range in Fig. 3b, at 3.8, 3, and 5 eV, respectively. A is the allowed optical transition in the parallel polarization and show the transition from HOMO-2 to LUMO+7. B and C indicate the transition from HOMO-4 to LUMO+4 and HOMO-7 to LUMO+1, respectively, in the perpendicular polarization, which are shown by arrows in Fig. 1.

All other optical constants that depend on the frequency can be obtained from the complex dielectric tensor components. Another important response function is the energy-loss function given as:

$$L_{ij}(\omega) = -\mathrm{Im}\left(\frac{1}{\varepsilon_{ij}(\omega)}\right) = \frac{\varepsilon''_{ij}(\omega)}{\varepsilon'_{ij}2(\omega) + \varepsilon''_{ij}2(\omega)}. \quad (5)$$

And the reflectivity at normal incidence is:

$$R_{ij}(\omega) = \frac{(n-1)^2 + k^2}{(n+1)^2 + k^2}, \quad (6)$$

where n and k are the real and imaginary parts of the complex refractive index, which are known as the refractive index and the extinction coefficient, respectively, given by the following relations:

$$n_{ij}(\omega) = \sqrt{\frac{\left|\varepsilon_{ij}(\omega) + \mathrm{Re}\varepsilon_{ij}(\omega)\right|}{2}}, \quad (7)$$

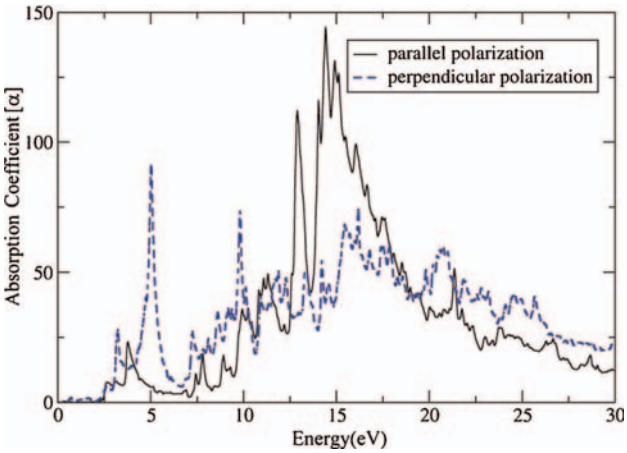

Figure 4 (online colour at: www.pss-b.com) The absorption coefficient of a (4,1) nanotube, for both polarizations, parallel and perpendicular to the tube axis.

$$k_{ij}(\omega) = \sqrt{\frac{\left|\varepsilon_{ij}(\omega) - \mathrm{Re}\varepsilon_{ij}(\omega)\right|}{2}}. \quad (8)$$

Also, the absorption coefficient and the real part of the optical conductivity are defined as:

$$\alpha_{ij}(\omega) = \frac{2\omega k_{ij}(\omega)}{c} = \frac{\omega\varepsilon''_{ij}(\omega)}{c\, n_{ij}(\omega)}. \quad (9)$$

$$\mathrm{Re}\sigma_{ij}(\omega) = \frac{\omega}{4\pi}\mathrm{Im}\varepsilon_{ij}(\omega), \quad (10)$$

where c is the velocity of light.

Figure 4 shows the absorption coefficient of a (4,1) nanotube, for both polarizations, parallel and perpendicular to the tube axis. The first peak appears when the absorption coefficient is about 2.6 eV. The maximum of absorption occurs at energy of 15 eV for the parallel polarization, which is related to the optical transition from HOMO-19 to LUMO+26, and for perpendicular polarization at energy 5 eV, related to the optical transition from HOMO-7 to LUMO+1. According to Eq. (9), the absorption coefficient is proportional to both the extinction coefficient and the imaginary part of the dielectric function, as can be seen in Figs. 3–5.

The reflectivity and refractive index of a (4,1) nanotube that are calculated, according to Eqs. (6) and (7), are shown

Table 2 First optical transitions (optical gaps, eV) in small-diameter SWCNTs.

(n,m)	(GGA) [this work]	LDA [32]	LDA [16]	GW [16]	BS [16]	exp. [9]	tube length (Å)	diameter (Å)	electric behavior
(3,3)[a]	3.0	2.8	2.83	3.26	3.17	3.1	2.46	4.07	metallic
(4,2)[a]	1.8	1.9	–	–	–	2.1	11.28	4.15	semiconducting
(4,1)	2.6	–	–	–	–	–	6.51	3.6	metallic
(5,0)	–	1.2	1.13	1.30	1.33	1.37	4.26	3.92	metallic

[a]The details of calculations are not included in this paper.

© 2010 WILEY-VCH Verlag GmbH & Co. KGaA, Weinheim

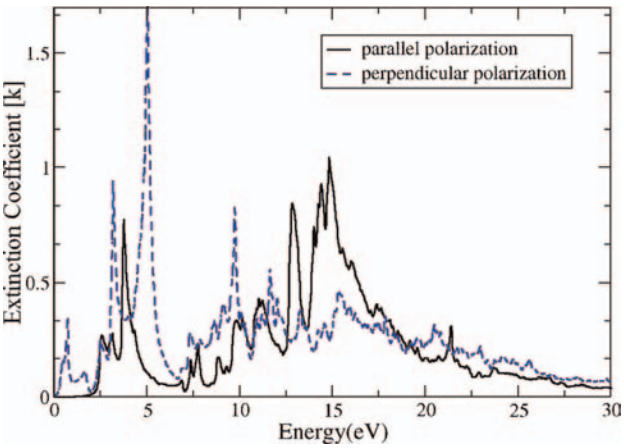

Figure 5 (online colour at: www.pss-b.com) The extinction coefficient of a (4,1) nanotube, for both polarizations, parallel and perpendicular to the tube axis.

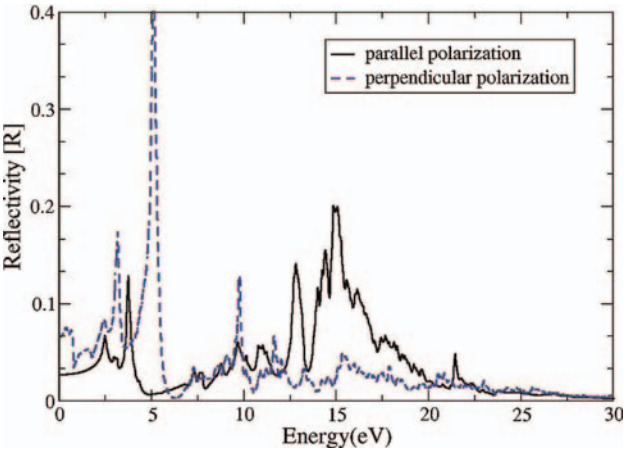

Figure 6 (online colour at: www.pss-b.com) The reflectivity of a (4,1) nanotube for both polarizations, parallel and perpendicular to the tube axis.

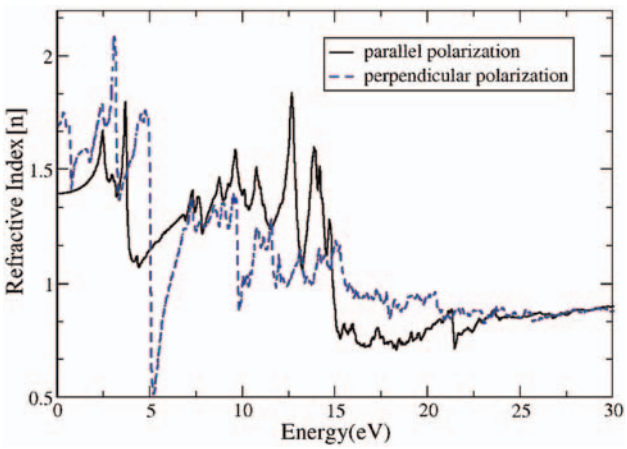

Figure 7 (online colour at: www.pss-b.com) The refractive index of a (4,1) nanotube for both polarizations, parallel and perpendicular to the tube axis.

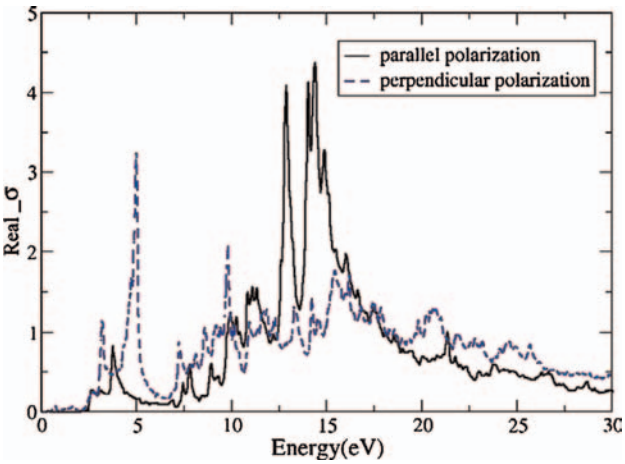

Figure 8 (online colour at: www.pss-b.com) The real part of the optical conductivity of a (4,1) nanotube for both polarizations, parallel and perpendicular to the tube axis.

in Figs. 6 and 7, respectively. Zeng et al. [33] have measured and discussed the reflectance of the bulk highly oriented pyrolytic graphite (HOPG) that arises from serial reflections of many graphene layers. While, in the case of SWNTs, only a single layer of graphene cylinder contributes to the total reflection. This implies that SWNTs can efficiently screen electromagnetic waves at resonant conditions. The refractive index at energies 15 and 5 eV are minimum for parallel and perpendicular polarization, respectively, where the absorption is maximum.

The calculated results for the real part of the optical conductivity of a (4,1) nanotube, for both polarizations, are shown in Fig. 8. The optical conductivity starts at the onset of the optical gap. The real part of the optical conductivity is proportional to the imaginary part of the dielectric function, in accordance with Eq. (10). The maximum of optical conductivity occurs at an energy of 5 eV for the perpendicular polarization and 15 eV for the parallel polarization.

3.2.1 Electron energy-loss spectroscopy (EELS) EELS is a valuable tool for investigating various aspects of materials [34]. It has the advantage of covering the complete energy range including nonscattered and elastically scattered electrons (zero loss), electrons that excite an atom's outer shell (valence loss), or valence interband transitions. In addition, the fast electrons excite the inner-shell electrons (core loss) or induce core-level excitation of near-edge structure (ELNES) and XANES. In the case of interband transitions, this consists mostly of plasmon excitations. The scattering probability for volume losses is directly connected to the energy-loss function.

In this work the loss function of a (4,1) nanotube for the both polarizations, parallel and perpendicular to the tube axis, have been calculated and the results are shown in Fig. 9. According to Eq. (5), the loss function is proportional to the imaginary part of the dielectric function, which is obvious in Figs. 3 and 9.

© 2010 WILEY-VCH Verlag GmbH & Co. KGaA, Weinheim

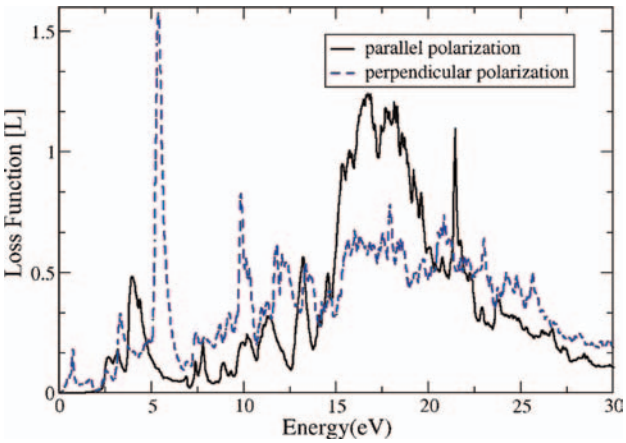

Figure 9 (online colour at: www.pss-b.com) The electron energy-loss function of a (4,1) nanotube for both polarizations, parallel and perpendicular to the tube axis.

Table 3 Calculated optical constants of a (4,1) nanotube for the polarization parallel to the tube axis.

electronic dielectric constant, $\varepsilon(\infty)$	refractive index constant, n	plasmon energy (eV)
1.98	1.4	3.919

The calculated energy-loss function show a sharp π electron plasmon peak at about 5 eV and a broad $\pi+\sigma$ electron plasmon peak around 15–22 eV.

The first highest peak value in Fig. 9 for the parallel polarization is obtained at about 3.919 eV for the plasmon energy. Table 3 shows the calculated optical constants of a (4,1) nanotube for the polarization parallel to the tube axis.

Now we consider the intraband transitions contribution in addition to interband transitions in the optical properties of a (4,1) nanotube. Adding the intraband transitions

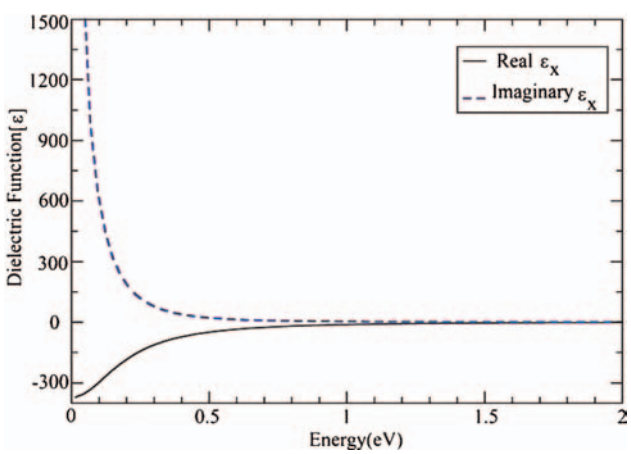

Figure 10 (online colour at: www.pss-b.com) Imaginary and real parts of the dielectric function considering the intraband contribution, in addition to the interband one, for polarization parallel to the tube axis.

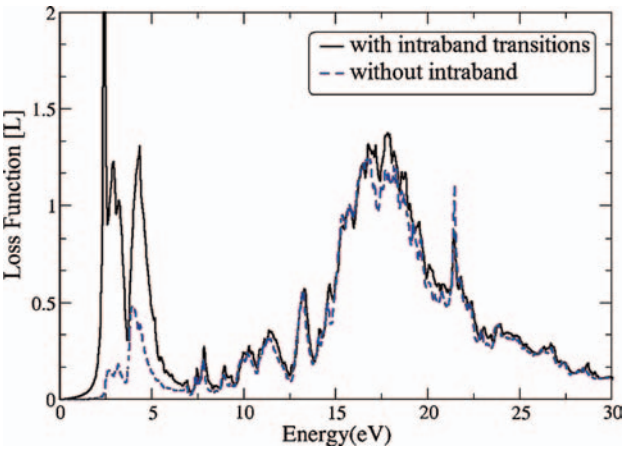

Figure 11 (online colour at: www.pss-b.com) Comparison of the energy-loss function of a (4,1) nanotube considering the intraband transitions contribution and without the intraband one for polarization parallel to the tube axis.

contribution, the optical spectra of a (4,1) nanotube will change significantly for the parallel polarization to the tube axis, while in the perpendicular polarization the optical spectra do not change. Figures 10–14 show the optical spectra of a (4,1) nanotube by considering the intraband transitions contribution. These figures show that for the polarization perpendicular to the tube axis, adding the intraband transitions does not have any effect on the optical spectra. By considering the intraband transitions contribution, the imaginary and real parts of the dielectric function have a singularity at zero frequency, as can be seen in Fig. 10.

3.2.2 Oscillator strength sum rule Another way to consider the number of electrons involved in the valence interband transition is to evaluate the sum rules. In principle, the optical sum rules provide a useful guide to interpreting

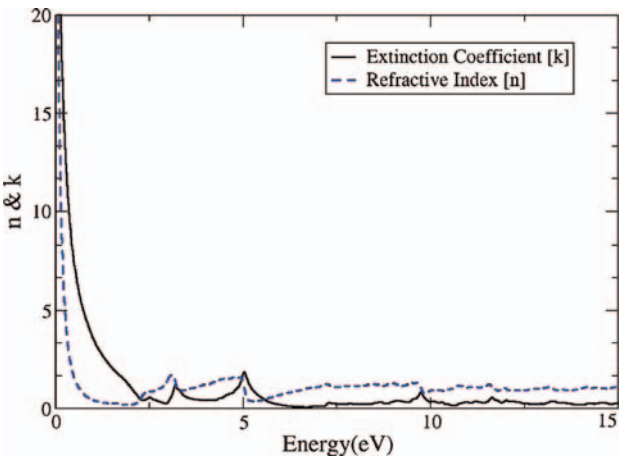

Figure 12 (online colour at: www.pss-b.com) Extinction coefficient and refractive index of a (4,1) nanotube, considering the intraband contribution, in addition to the interband one, for polarization parallel to the tube axis.

© 2010 WILEY-VCH Verlag GmbH & Co. KGaA, Weinheim

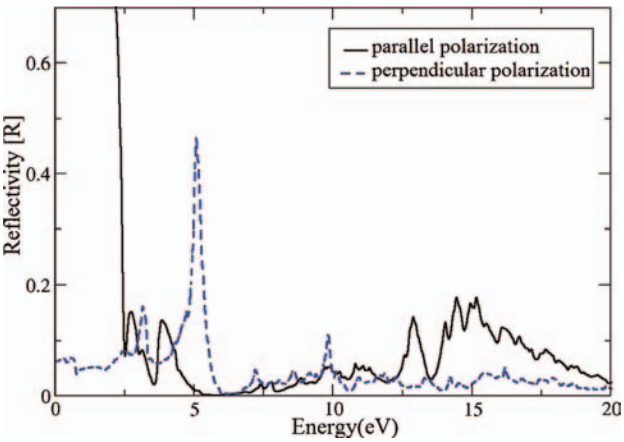

Figure 13 (online colour at: www.pss-b.com) The reflectivity of a (4,1) nanotube considering the intraband contribution, in addition to the interband one, for both polarizations, parallel and perpendicular to the tube axis.

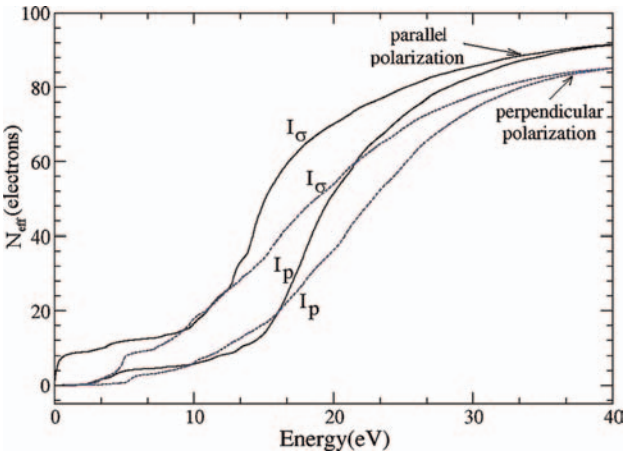

Figure 15 Sum rule of the optical conductivity, I_σ, and of the energy-loss function, I_p, by carrying out the integrations given in Eqs. (11) and (12) as a function of energy, for both polarizations.

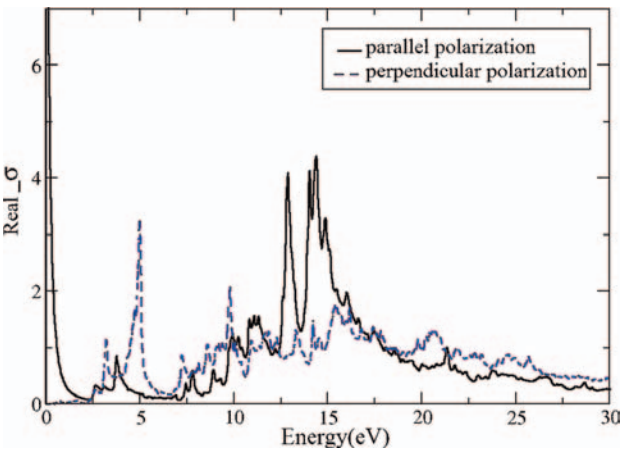

Figure 14 (online colour at: www.pss-b.com) The real part of the optical conductivity of a (4,1) nanotube considering the intraband contribution, in addition to the interband one, for both polarizations.

the experimental results and could be used in order to check the consistency of optical data. There are two kinds of optical sum rules, which give information about the absorption process [31]:

$$I_\sigma = \int_0^{\omega'} \mathrm{Im}\varepsilon(\omega)\omega \mathrm{d}\omega = 4\pi \int_0^{\omega'} \mathrm{Re}\sigma(\omega)\mathrm{d}\omega = N_{\mathrm{eff}}(\omega') \tag{11}$$

and

$$I_\mathrm{p} = \int_0^{\omega'} \mathrm{Im}\left(\frac{-1}{\varepsilon(\omega)}\right)\omega \mathrm{d}\omega = N_{\mathrm{eff}}(\omega'). \tag{12}$$

The sum rules I_σ and I_p calculated from Eqs. (11) and (12) describe rather different processes and in fact differ significantly as a function of energy. The sum rule, I_σ, is related to the rate of energy absorption (photons) by transverse fields (photons) in the system. The sum rule on the electron loss functions, I_p, is the rate of energy absorption by the longitudinal fields (electrons) [30]. In fact, the intraband oscillator strength is measured by I_σ and I_p is related to plasma excitations. However, the saturation value of both I_σ and I_p should be the same. In the low-energy region, the contribution to the intraband spectrum should sum up to the number of the outermost valence electrons.

We have calculated sum rules for (4,1) nanotube according to Eqs. (11) and (12) for both polarizations, parallel and perpendicular to the tube axis, as shown in Fig. 15.

The saturation values of I_σ, and I_p at an energy of 40 eV are, for both parallel and perpendicular polarization, 91.4 and 85, respectively. The effective number of electrons for the parallel polarization is more than that in the perpendicular polarization.

4 Conclusions We have calculated the electronic structure and optical spectra of a chiral (4,1) nanotube considering the intraband in addition to the interband transitions contribution for both polarizations, parallel and perpendicular to the tube axis. The calculated optical gap, electronic dielectric constant, and the refractive index in the parallel polarization are obtained 2.6, 1.98, and 1.4 eV, respectively. The maximum amount of optical conductivity occurs at energies of 5 and 15 eV for the polarizations perpendicular and parallel to the tube axis, respectively. At these energies the values of absorption are maximum. Adding the intraband transition contributions showed that the dielectric function has a singularity at zero frequency, due to the metallic behavior of a (4,1) chiral nanotube. By

© 2010 WILEY-VCH Verlag GmbH & Co. KGaA, Weinheim

considering the intraband transitions contribution, the change of optical spectra of a (4,1) nanotube for the parallel polarization to the tube axis is significant, while for the polarization perpendicular to the tube axis it does not have any effect on the optical spectra.

References

[1] S. Iijima, Nature **354**, 56–58 (1991).
[2] S. Tasaki, K. Maekawa, and T. Yamabe, Phys. Rev. B **57**, 9301–9318 (1998).
[3] I. Bozovic, N. Bozovic, and M. Damnjanovic, Phys. Rev. B **62**, 6971–6974 (2000).
[4] O. E. Alon, V. Averbukh, and N. Moiseyev, Phys. Rev. Lett. **85**, 5218–5221 (2000).
[5] E. L. Ivchenko and B. Spivak, Phys. Rev. B **66**, 155404–155409 (2002).
[6] R. Saito, G. Dresselhaus, and M. S. Dresselhaus, Physical Properties of Carbon Nanotubes (Imperial College Press, London, 1998).
[7] M. S. Dresselhaus, G. Dresselhaus, and P. C. Eklund, Science of Fullerenes and Carbon Nanotubes (Academic Press, San Diego, CA, 1996).
[8] S. M. Bachilo, M. S. Strano, C. Kittrell, R. H. Hauge, R. E. Smalley, and R. B. Weisman, Science **298**, 2361–2366 (2002).
[9] Z. M. Li, Z. K. Tang, H. J. Liu, N. Wang, C. T. Chan, R. Saito, S. Okada, G. D. Li, J. S. Chen, N. Nagasawa, and S. Tsuda, Phys. Rev. Lett. **87**, 127401 (2001).
[10] M. J. O'Connell, S. M. Bachilo, C. B. Huffman, V. C. Moore, M. S. Strano, E. H. Haroz, K. L. Rialon, P. J. Boul, W. H. Noon, C. Kittrell, J. Ma, R. H. Hauge, R. B. Weisman, and R. E. Smalley, Science **297**, 593–596 (2002).
[11] J. Deslippe, M. Dipoppa, D. Prendergast, M. V. O. Moutinho, R. B. Capaz, and S. G. Louie, Nano Lett. **9**, 1330–1334 (2009).
[12] X. Zhao, Y. Liu, S. Inoue, T. Suzuki, R. O. Jones, and Y. Ando, Phys. Rev. Lett. **92**, 125502 (2004).
[13] Z. K. Thang, J. P. Zhai, Y. Y. Tong, X. J. Hu, R. Saito, Y. J. Feng, and Sheng. Ping, Phys. Rev. Lett. **101**, 047402 (2008).
[14] R. Scipioni, Phys. Status Solidi B **244**(9), 3137–3142 (2007).
[15] J. Deslippe, C. D. Spataru, D. Prendergast, and S. G. Louie, Nano Lett. **7**, 1626–1630 (2007).
[16] C. D. Spataru, S. Ismail-Beigi, L. X. Benedict, and S. G. Louie, Phys. Rev. Lett. **92**, 077402 (2004).
[17] E. Chang, G. Bussi, A. Ruini, and E. Molinari, Phys. Rev. Lett. **92**, 196401 (2004).
[18] A. G. Marinopoulos, L. Reining, A. Rubio, and N. Vast, Phys. Rev. Lett. **91**, 046402 (2003).
[19] A. G. Marinopoulos, L. Wirtz, A. Marini, V. Olevano, A. Rubio, and L. Reining, Appl. Phys. A **78**, 1157–1167 (2004).
[20] P. Blaha, D. Singh, P. I. Sorantin, and K. Schwarz, Phys. Rev. B **46**, 1321–1325 (1992).
[21] J. P. Perdew, J. A. Chevary, S. H. Vosko, K. A. Jackson, M. R. Pederson, D. J. Singh, and C. Fiolhais, Phys. Rev. B **46**, 6671–6687 (1992).
[22] M. Peterson, F. Wanger, L. Hufnagel, M. Scheffler, P. Blaha, and K. Schwarz, Comput. Phys. Commun. **126**, 294–309 (2000).
[23] P. Blaha and K. Schwarz, WIEN2k, http://www.wien2k.at/, Vienna University of Technology Austria (2002).
[24] R. Saito, G. Dresselhaus, and M. S. Dresselhaus, Phys. Rev. B **61**, 2981–2990 (2000).
[25] G. Bertoni and L. Calmels, Micron **37**, 486–491 (2006).
[26] W. A. de Heer, W. S. Bacsa, A. Chatelain, T. Gerfin, R. Humphrey-Baker, L. Forro, and D. Ugarte, Science **268**, 845–847 (1995).
[27] R. Kuzuo, M. Terauchi, and M. Tanaka, Jpn. J. Appl. Phys. **31**, 1484–1487 (1992).
[28] F. Bommeli, L. Degiorgi, P. Wachter, W. S. Bacsa, W. A. de Heer, and L. Forro, Solid State Commun. **99**, 513–517 (1996).
[29] M. Ichida, S. Mizuno, Y. Tani, Y. Saito, and A. Nakamura, J. Phys. Soc. Jpn. **68**, 3131–1333 (1999).
[30] F. Wooten, Optical Properties of Solids (Academic Press, New York, 1972), chap. 6.
[31] C. Ambrosch-Draxl and J. O. Sofo, Comput. Phys. Commun. **175**, 1–14 (2006).
[32] H. J. Liu and C. T. Chan, Phys. Rev. B **66**, 115416 (2002).
[33] H. Zeng, L. Jiao, X. Xian, X. Qin, Zh. Liu, and X. Cui, Nanotechnology **19**, 045708–045712 (2008).
[34] S. Loughin, R. H. French, L. K. Noyer, W. Y. Ching, and Y. N. Xu, J. Phys. D **29**, 1740–1750 (1996).

© 2010 WILEY-VCH Verlag GmbH & Co. KGaA, Weinheim